Proceedings of the ASME 2022
International Design Engineering Technical Conferences and
Computers and Information in Engineering Conference
IDETC/CIE2022
August 14-17, 2022, St. Louis, Missouri

DETC2022-91021

SPATIAL-TEMPORAL MODELING USING DEEP LEARNING FOR REAL-TIME MONITORING OF ADDITIVE MANUFACTURING

Hyunwoong Ko
Arizona State University, AZ, USA

Jaehyuk Kim
Associate, National Institute of Standards and Technology, MD, USA
Pohang University of Science and Technology, Republic of Korea

Yan Lu
National Institute of Standards and Technology, MD, USA

Dongmin Shin
Hanyang University, Republic of Korea

Zhuo Yang
Associate, National Institute of Standards and Technology, MD, USA
University of Massachusetts Amherst, MA, USA

Yosep Oh
Kyonggi University, Republic of Korea

ABSTRACT

Real-time monitoring for Additive Manufacturing (AM) processes can greatly benefit from spatial-temporal modeling using deep learning. However, existing, deep-learning approaches in AM are case-dependent, and therefore not robust to changes of control inputs and data types. As AM is dynamic and complex, this limitation leads to a lack of systematic, DL approaches for real-time monitoring of AM, which involves a large number of varying control parameters and monitoring data. To address the challenge, this paper introduces a novel approach for developing spatial-temporal models to monitor Laser Powder Bed Fusion (LPBF) processes using deep learning on real-time, monitoring data. First, we present a novel model for representing in-situ-monitoring and control data of LPBF at multiple scales. Second, from the model, we extract spatial-temporal relationships for in-situ monitoring of LPBF processes. Third, we present a spatial-temporal, modeling approach using the architecture of convolutional long short-term memory (LSTM) to monitor the spatial-temporal relationships and detect anomalies. A case study used convolutional LSTM Autoencoder on optical, melt-pool-monitoring data, one of the most widely adopted data types in in-situ monitoring of LPBF. The data was generated from an LPBF testbed called the Additive Manufacturing Metrology Testbed. The novel, learning approach enables spatial-temporal modeling of AM dynamics directly from real-time data for the monitoring of varying AM environments. This methodical approach provides the potential to fuse real-time data at multiple, spatial-temporal scales.

Keywords: Deep Learning, Laser Powder Bed Fusion, Spatial-temporal Modeling, Real-time

1. INTRODUCTION

Additive Manufacturing (AM)'s unique capabilities have promised unprecedented opportunities to improve product performance and to flexibly react to the changes of desired product designs and functions [1]. Despite this promise, there still is a lack of knowledge about AM's dynamics in complex processes (e.g., powder melting or melt-pool solidification in Laser Powder Bed Fusion (LPBF) and Directed Energy Deposition (DED) processes) [2]. This means that costly post-build inspection or functional testing is required to qualify components for end-use applications [3]. Understanding the AM processes in real time helps with identifying their impacts on the quality of the final products (e.g., surface roughness and porosity). Therefore, real-time monitoring provides evidence for improved quality and process control of born-qualified products [2].

Real-time monitoring measures process signatures, so called the voice of the process, to acquire dynamic, material-evolution

data that give information about both process physics and part quality metrics [4]. The acquisition of such in-situ data has suggested a place for data-driven models with the potential to be much faster and realistic than their simulated counterparts [3]. The data-driven models based on the real-time, real-world data could lead to advanced, on-line monitoring of dynamics in AM processes.

Deep learning (DL) has demonstrated remarkable promise in the data-driven modeling for AM. Especially using real-time monitoring data, a DL model learns dynamics of AM process [2]. The DL methods using in-situ-monitoring data make predictions about flaws or porosity with considering the dynamic nature of the AM processes [4]. In DL for AM, spatial and temporal modeling is required to understand and control AM processes at multiple scales. As AM is dynamic and complex, there are a large number of varying control parameters at multiple, spatial-temporal scales in AM [5]. To monitor AM processes and detect faults in real time, an approach for DL modeling needs to be robust to spatial-temporal changes in controls and data types.

Many DL-based, modeling methods, however, are control-input- or data-type dependent, and therefore ad-hoc and not robust to control and data changes. A problem is that the high diversity in AM control parameters enables collecting enough data to develop DL models for each process parameter set. This limits the development of a generic approach to create DL models in a dynamic AM environment. Such limitation leads to false detections increasingly, as useful information about the process dynamics is not applicable when using DL models as well as the knowledge extracted from the DL models or applying modeling approaches for different types of data or AM environments.

To address the challenge, this study presents a novel approach for spatial-temporal modeling using DL for real-time monitoring of AM dynamics. We newly represent data of process control and monitoring in AM - where a list of sequential observations from monitoring is present with controlled inputs – that characterize relationships between the monitoring-control elements and identify relationships specific to real-time-monitoring data. Then, we present an approach to map the extracted representations to the data-driven, predictive models as modeling inputs. This study uses convolutional Long Short-term Memory (ConvLSTM), which is known for learning from spatial-temporal data [6]. Our approach newly enables spatial-temporal modeling using DL in a way robust to control and data changes for in-situ monitoring of AM. This study mainly focuses on LPBF, one of the most widely adopted metallic, AM processes.

The remainder of the paper is as follows. Section 2 introduces the approach. Section 3 demonstrates a case study. Section 4 presents results and discussions. Following this, we conclude this article in Section 5 with concluding remarks and future work.

2. APPROACH

In this section, we present a novel approach for developing spatial-temporal models to monitor AM processes using DL on real-time data, as shown in FIGURE 1. First, we present a novel, formal representation of in-situ-monitoring and control data in LPBF. Second, using the representation, we extract and structure spatial-temporal relationships considered for real-time monitoring of LPBF processes. Lasty, we design a spatial-temporal model based on the architecture of convolutional LSTM autoencoder.

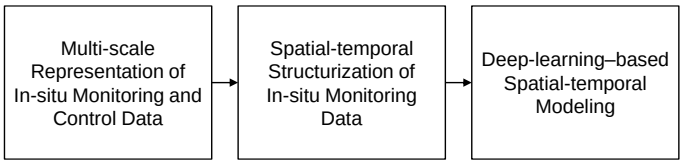

FIGURE 1: AN OVERVIEW OF THE SPATIAL-TEMPORAL MODELING USING DL FOR REAL-TIME MONITORING OF AM DYNAMICS

2.1 A Multi-scale Representation of In-situ-Monitoring and Control Data

We present a novel, formal representation of the data of in-situ monitoring and control of LPBF as shown in FIGURE 2. LPBF includes multiple processes that transform a virtual product description to a physical, final part by applying laser to powder materials in layer-by-layer manners. Therefore, LPBF can be considered a function that maps a design specification into a realized tangible product with controls. Considering that, the representation is developed for the function as a set of certain series of states as well as associated controls to the goal in the final state. It consists of a series of procedures that transform a current part state into a next state by exercising a control on AM parameters at each step.

A model for LPBF can break down as follows: models representing powder-bed raking, behaviors in and around melt pools, and other sub-LPBF-processes [7]. A central aim of digital representations of LPBF using data is to present an integrated, layer-wise, multi-scale representation. In this study, to represent in-situ part states in LPBF, there are two types of state transitions defined: layer-wise and inner-layer transitions.

In LPBF, for each layer, a machine deposits and presses down a new layer of powder for powder feeding. The layer-wise transition represents each actualization of such control events that change the layers. Equation (1) captures this transition function as follows.

$$\delta^{ext}: X^{ext} \times \sum^{ext} \rightarrow X^{ext} \quad (1)$$

In Equation (1), X^{ext} is a set of states representing each layer, where $\sum^{ext}$ is a set of controls for proceeding from a completed layer to a next layer, which includes powder feeding and powder-bed raking. Each actualization of a control in this transition function is defined as a state transition δ^{ext}. δ^{ext} is a transition

function representing the layer-wise transitions using the two inputs of previous states and control events in $X^{ext} \times \sum^{ext}$.

On the other hand, the inner-layer transition is related to melting powders by laser scanning and solidifying melted powders in a layer. This transition reflects the observations and controls of each layer's building operation from start to finish. The inner-layer transition has two types: the transitions by control and time advance. The inner-layer transition by control represents a layer's state changes as a laser beam melts powders and melted powders are solidified. This transition is captured in Equation (2).

$$\delta^{int}: X^{int} \times \sum^{int} \rightarrow X^{int} \tag{2}$$

In Equation (2), X^{int} is a set of states that represent a LPBF build being processed within a layer, where $\sum^{int}$ is a set of controls to complete a layer such as layer scanning and part solidification. Each actualization of a control in this transition function is defined as a state transition δ^{int}. δ^{int} is a transition function that represents the inner-layer transitions using the two inputs of previous states and control events in $X^{int} \times \sum^{int}$.

In LPBF, thermo-dynamics, hydro-dynamics, and fluid-dynamics primarily drive the creation of powders' or melted powders' properties and their dependencies [2]. We call an entity that has such properties while participating in a physical, LPBF process a physical, real entity (e.g., metallic powders, melt pools: portions of melted powders) [2]. At any instance in time, any physical, real entity in a layer (e.g., i^{th} layer) exists in a physical state (e.g., i^{th} layer's j^{th} state after a series of laser scanning: $x_{i,j} \in X_{int}$, where $1 \leq i, j < \infty$). To digitally represent the physical properties, the properties of physical, real entities, with data, there are two types defined in AM: state and rate properties [2]. State property is a characterization of an amount or a momentum of a physical, real entity participating in an AM process. Rate property is a characterization of a flow rate, or a force applied to a physical, real entity during an AM process.

A state, which changes during an AM process (e.g., melt-pool size changes as laser is applied and laser nozzle moves), is affected by (1) preceded state properties of neighboring, physical entities (e.g., neighboring, metallic powders being melted and solidified) and (2) controls of the rate properties (e.g., laser frequency). The dependencies by the former and later are captured by the two types of inputs X^{int} and $\sum^{int}$, respectively, in $X^{int} \times \sum^{int}$ of Equation (2). Based on Equation (2), the model represents an interaction between the physical properties, which we call a dynamical dependency [2], participating in an AM process. An example of a dynamical dependency is the dependency of a melt-pool-volume state on a neighboring, melt track's state. This type of dependency between state properties is called a state-state dependency. Another example is the dependency of a melt-pool-volume state on laser frequency. This type between state and rate properties is called a state-rate dependency. Using data, the two types of the dynamical dependencies together represent mechanisms by which physical, real entities transfer or control the flow of energy among them,

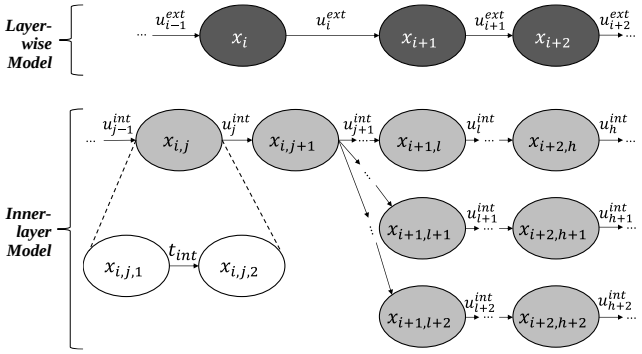

FIGURE 2: A GRAPHICAL REPRESENTATION OF IN-SITU MONITORING AND CONTROL DATA.

and therefore enable the evolvement of part states in LPBF processes.

The representation model also captures information about temporal measures of part states that are independent of the interaction between physical properties in LPBF processes. This information represents a measure that changes within a temporal coordinate system. Therefore, a part-state transition caused by temporal change is not necessarily involved in a dynamical dependency. The other type of inner-layer transition, transition by time advance, is represented in Equation (3) to capture those relationships using time advance function t_{int}.

$$\delta_{int}: X_{int} \times t_{int} \rightarrow X_{int} \tag{3}$$

2.2 Spatial-temporal Structurization of In-situ, Monitoring Data

The formal, data model newly defines the representation of all directed paths of observations and controls of a LPBF build as Equation (4).

$$U \in \sum^{*}: \delta(x_0, u) \tag{4}$$

U represents controls that actualize all state changes at both inner-layer and layer-wise levels, starting from the initial state x_0 of a build in the first layer. Equation (4) uses an extended transition function $\delta: X \times \sum^{*} \rightarrow X$, where $X = X^{ext} \cup X^{int}$, $\sum = \sum^{ext} \cup \sum^{int}$, and $\sum^{*}$ denotes a set of all concatenations of controls in $\sum$. In this way, a concatenation of controls represents successive controls, defined as a control activity, as an ordered sequence of finite operational control events. A control activity u is in U if and only if it corresponds to an admissible path in the state transition model, equivalently, if and only if δ^{ext} or δ^{int} is defined at $\delta(x_0, u)$.

Among the control activities in U, we define another set of control activities ma in Equation (5):

$$MU \coloneqq \{ma \in MU: \delta(x_0, mu) \in F\} \tag{5}$$

, where F is a set of final states. Therefore, Equation (5) represents all control activities in the scanning patterns, all

possible successive controls, for a LPBF build, which enable the state transitions representing the transformation of raw materials to a final part during a build process.

The successive controls in Equation (5) lead to corresponding successive changes of LPBF part states to monitor during the build process. Let x_i and x_{i+1} be two, successive states representing the states of neighboring layers where x_i is the precedent layer and x_{i+1} is the following layer. In this sense, the model represents targeted observations with a series of L states where a LPBF build is described as a concatenation of layer states in Equitation (6) as follows.

$$x = \prod_{i=1}^{L} x_i \,, 1 \le L < \infty \tag{6}$$

, where, $x = x_1 \cdot x_2 \cdot x_3 \cdot \cdots \cdot x_L$ such that $x_{i+1} = \delta^{ext}(x_i, u_i) = \delta^{ext}(\delta^{ext}(x_{i-1}, u_{i-1}^{ext}), u_i^{ext})$ and $u_{i-1}^{ext}, u_i^{ext} \in \sum^{ext}$.

x_i is represented as Equation (7). Equation (7) is a function of the model that captures the concatenations of inner-layer states in the transitions by inner-layer controls such as control of laser power, speed, location, and direction for laser scanning of powders and solidification of melted powders, to complete the build in the layer x_i from start to finish.

$$x_i = \prod_{j=1}^{M} x_{i,j} \,, 1 \le M < \infty \tag{7}$$

, where $x_i = x_{i,1} \cdot x_{i,2} \cdot x_{i,3} \cdot \cdots \cdot x_{i,M}$ such that $x_{i,j} = \delta^{int}(x_{i,j}, u_l^{int}) = \delta^{int}(\delta^{int}(x_{i,j-1}, u_{j-1}^{int}), u_j^{int})$ and $u_{j-1}^{int}, u_j^{int} \in \sum^{int}$.

Considering the transition between the inner states of $x_{i,j}$ by the time advance function t_{int}, $x_{i,j}$ is represented as Equation (8). Equation (8) is a function of the model that captures the concatenations of inner-layer states of x_i, especially $x_{i,j}$, changed by time advance.

$$x_{i,j} = \prod_{k=1}^{N} x_{i,j,k} \,, 1 \le N < \infty \tag{8}$$

, where $x_{i,j} = x_{i,j,1} \cdot x_{i,j,2} \cdot x_{i,j,3} \cdot \cdots \cdot x_{i,j,N}$ such that $x_{i,j,k+1} = \delta_{int}(x_{i,j,k}, t_{int}) = \delta_{int}(\delta_{int}(x_{i,j,k-1}, t_{int}), t_{int})$. Therefore, the in-situ, monitoring data of an LPBF build is represented as Equation (9) to include both layer-wise and inner-layer transitions.

$$\prod_{i=1}^{L} \prod_{j=1}^{M} \prod_{k=1}^{N} x_{i,j,k} \,, 1 \le L, M, N < \infty \tag{9}$$

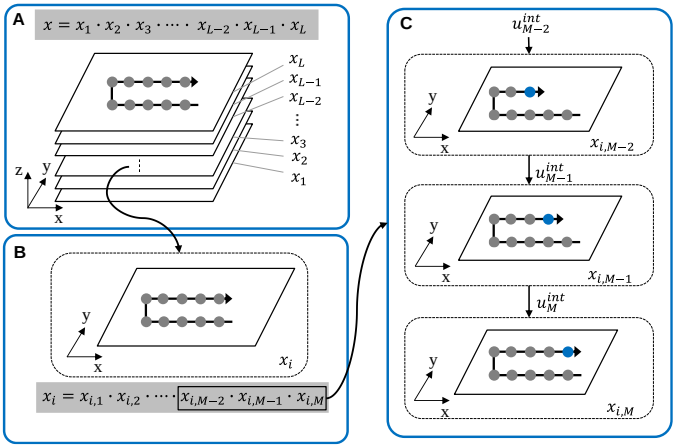

FIGURE 3: SPATIAL-TEMPORAL RELATIONSHIPS FOR IN-SITU MONITORING OF LPBF PROCESSES EXTRACTED FROM THE REPRESENTATION MODEL: A. A CONCATENATION OF LAYER-WISE STATE TRANSITION, B. A LAYER AS A CONCATENATION OF INNER-LAYER STATE TRANSITION, AND C. AN INNER-LAYER STATE TRANSITION BY LASER SCANNING (GRAY CIRCLES REPRESENT INNER-LAYER CONTROL POINTS. THE ARROWS ON THE LAYERS REPRESENT LASER-SCANNING DIRECTIONS. A BLUE CIRCLE REPRESENTS A CONTROL POINT THAT ACTUALIZES EACH STATE TRANSITION. FOR EXAMPLE, IN $X_{I,M-2}$ OF C, THE BLUE CIRCLE IS A CONTROL POINT WHERE U_{M-2}^{INT} HAPPENED TO ACTUALIZE THE STATE TRANSITION FROM THE PREVIOUS STATE TO THE STATE $X_{I,M-2}$)

Equation (9) represents spatial-temporal relationships extracted for in-situ monitoring of LPBF processes. The layer-wise, state transitions in an LPBF process always happen between physically, neighboring layers. The first layer (x_1 in FIGURE 3A) is followed by the second layer (x_2 in FIGURE 3A), which the third layer (x_3 in FIGURE 3A) follows, and this continues until the final layer (x_L in FIGURE 3A) of a LPBF build. Therefore, the spatial dependencies between the neighboring layers are measurable in the representation model for a real-time observation of an LPBF build, in addition to the temporal dependencies between the layers captured by the concatenations. FIGURE 4 shows an example of a spatial-temporal dependency between two, successive, neighboring layers with the layer-wisely interacting areas where the solidified areas after layer scanning in the Layer *i-1* are remelted by layer scanning in the Layer *i*. This example shows a dependency of a melt-pool volume on a neighboring, previous layer's state. Examples of the previous layer's state is the energy density or volume of melted and solidified areas in the interacting areas of the previous layer, which the model captures in the layer-wise transition function for in-situ monitoring.

The model also captures the spatial-temporal dependencies between neighboring, melt pools within a layer. The concatenations of the inner-layer states generated by the state transitions can be based on the successive control inputs for a layer (example of u_{M-2}^{int}, u_{M-1}^{int}, and u_M^{int} shown in FIGURE 3 which can be controls of laser power, location, direction, and

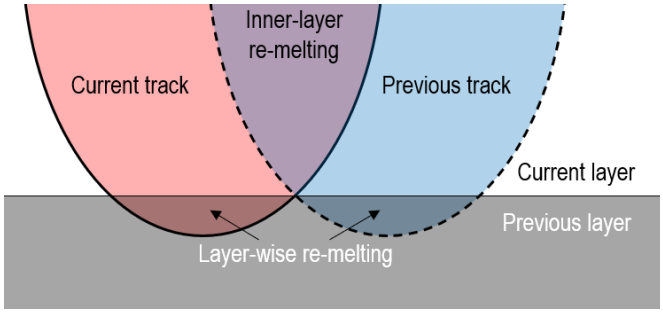

FIGURE 4: AN EXAMPLE OF LAYER-WISE AND INNER-LAYER DEPENDENCIES BETWEEN MELT-POOL STATES IN LPBF

speed in a layer). Such control creates successive, neighboring, melt pools and tracks in a layer. Therefore, the concatenations in Equation (9) capture the spatial-temporal dependencies between the melt pools: the relationships of the states of successive, neighboring, melt pools and tracks. FIGURE 4 also shows an example of a spatial-temporal dependency between two, successive, neighboring melt pools within a layer of which the interacting area is remelted. This example shows a dependency of a melt-pool volume on the state of a neighboring, previous melt pool within a layer, such as its energy density and volume of melted and solidified areas, especially in the interacting areas. This time the model captures an interaction in the inner-layer transition.

2.3 Deep-learning-based, Spatial-temporal Modeling

For spatial-temporal modeling, we additionally adopt Convolutional LSTM (ConvLSTM) neural network. Based on Equation (9), structured, monitoring data can contain information on a spatial state of a LPBF build in a temporal order. For example, $x_{i,j,k}$ in Equation (9) can be a two-dimensional representation of a spatial state of a build: a spatial-state information represented by a matrix with $m \times n$ elements. An example of $x_{i,j,k}$, in this case, is an image capturing information on a spatial state of a layer of a build such as a geometry of a melt-pool track of a layer. Then, $a_{ij} \in x_{i,j,k}$ becomes a value of the spatial information of $i \times j$ position in $x_{i,j,k}$. Based on such representation of $x_{i,j,k}$, the concatenation in Equation (9) can represent a whole, LPBF build at multiple, spatial-temporal scales. Those data then become inputs to a ConvLSTM model for spatial-temporal prediction of LPBF dynamics.

ConvLSTM can be represented as Equations (10)~(15) [6].

$$i_t = \sigma(W_{Xi} * X_t + W_{Hi} * H_{t-1} + W_{Ci} \odot C_{t-1} + b_{Hi}) \quad (10)$$
$$f_t = \sigma(W_{Xf} * X_t + W_{Hf} * H_{t-1} + W_{cf} \odot C_{t-1} + b_f) \quad (11)$$
$$g_t = \tanh(W_{Xg} * X_t + W_{Hg} * H_{t-1} + b_{h\_g}) \quad (12)$$
$$C_t = f_t \odot C_{t-1} + i_t \odot g_t \quad (13)$$
$$o_t = \sigma(W_{Xo} * X_t + W_{Ho} * H_{t-1} + W_{Co} \odot C_t + b_{f\_o}) \quad (14)$$
$$\mathcal{H}_t = o_t \odot \tanh(C_t) \quad (15)$$

The ConvLSTM can use convolution filters of different sizes to capture spatial-temporal dependencies at different scales. We can regard all the inputs based on the structured input data ($\{X_1, \cdots, X_t\} \subset \{x_{1,1,1}, \cdots, x_{L,M,N}\}$, cell outputs $\{C_1, \cdots, C_t\}$, hidden states $\{H_1, \cdots, H_t\}$, and the input, forget, and output gates i_t, f_t, and o_t, respectively, of the ConvLSTM as 3D tensors. The first two dimensions of the 3D tensors are spatial dimensions. The last dimension of the 3D tensors is the temporal dimension. The outputs of ConvLSTM cells depend on the inputs and actual states of local neighbors following the data representation model presented in Section 2.1 and Section 2.2. In Equations (10)~(15), '$*$' represents the convolution operator, '$\odot$' represents the Hadamard product, and '$\sigma(\cdot)$' represents the logistic sigmoid function.

3. CASE STUDY

The aim of the case study is to assess the proposed modeling approach. Specifically, we test an anomaly detection task, which is to detect the anomalous melt pools with the spatial-temporal, modeling approach. We consider a semi-supervised method, especially AutoEncoder, which can learn a meaningful representation into semi-labeled input data. The anomaly detection using AutoEncoder has typically three steps: 1) to define a normal input 2) to develop an Autoencoder model, and 3) to monitor an anomaly score. Autoencoder is trained with the only defined normal input, and a residual between an input and a reconstructed input, is used as the anomaly score, which means how different from normal input. We explain them in more detail in the sub-sections.

3.1 Experimental Design

An experiment is carried out using the Additive Manufacturing Metrology Testbed (AMMT) at the National Institute of Standards and Technology (NIST), which is an open-platform laser bed fusion system. This experiment creates 5mm x 9mm x 5mm geometry of a part on a wrought nickel alloy 625 (IN625) plate cut to 100mm x 100mm x 12.5mm. A commanded laser power is 100 W and scan speed is 900mm/s for a pre-contour and infill hatching occurred at 195 W and 800mm/s respectively. The part consists of 250 layers with 20μm thickness and 90° rotation between layers. The co-axial melt pool monitoring (MPM) camera is optically aligned with a laser. The camera generates melt-pool images with a 100μs/frame sampling rate. These images are 120 × 120 pixels and have gray-scale pixels whose range is 0 to 255, where each pixel is 8 x 8μm. Detailed experiment descriptions can be found in [8].

3.2 Data Structurization and Pre-processing

We use 5226 melt-pool images from layer 210 for training the model, and 4065 images from layer 150, which has many anomaly cases, for testing. These images are initially 120 × 120 pixels in size. These are cropped to 60 × 60 pixels around the peak pixel values. To reduce discrete noises, their pixel values are subtracted by the 10-pixel value. A melt-pool image represents a local change of a spatial state of a layer as shown in the top of FIGURE 5. To add temporal dependencies, the concatenations of melt-pool images, following Equation (9), become input for the DL model. In this study, we set 4-time

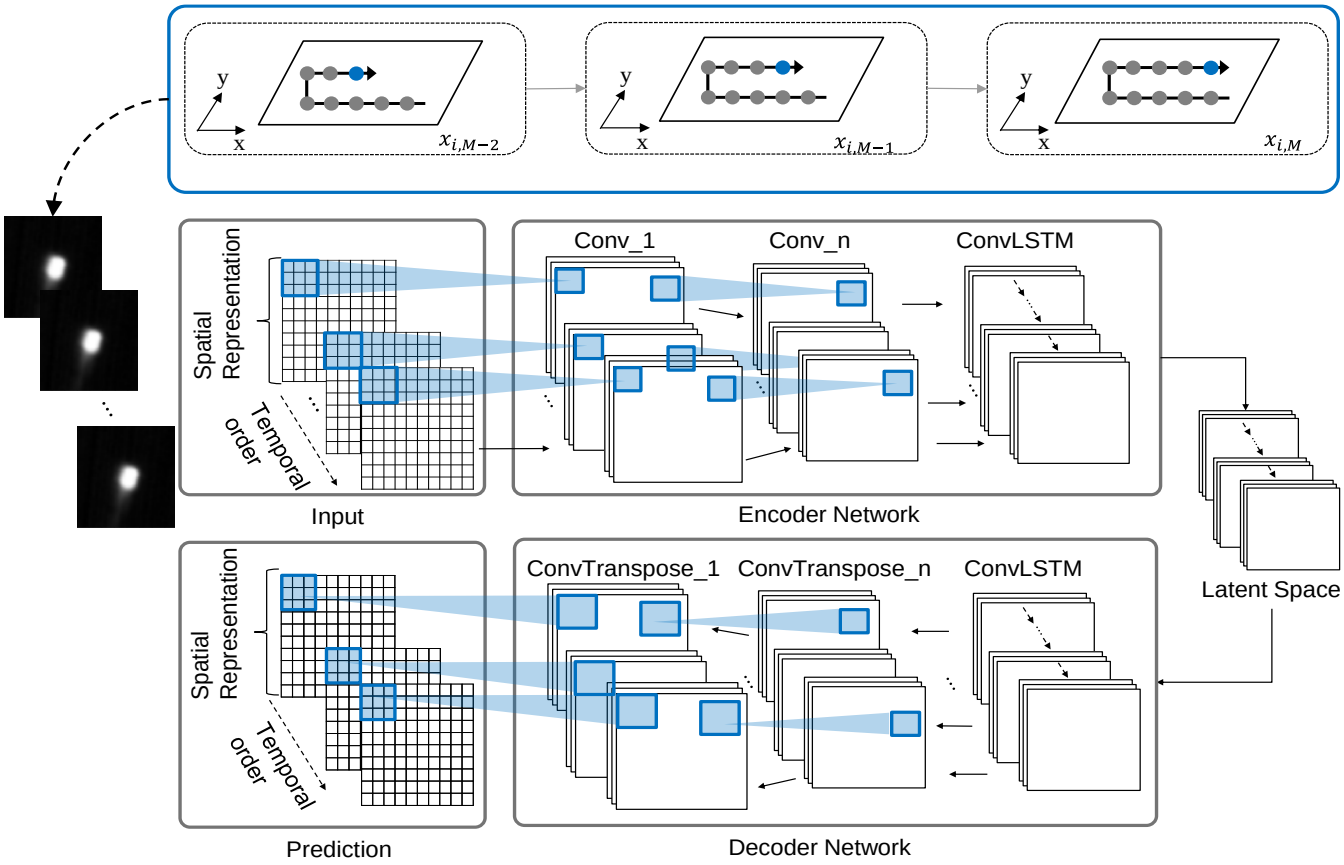

FIGURE 5: A CONVOLUTIONAL-LSTM-AUTOENCODER ARCHITECTURE WITH MELT-POOL IMAGE CONCATENATIONS STRUCTURED BASED ON EQUATION (9)

windows and 1-sliding; thus, 3,975 concatenations and 442 concatenations are used for training and validation, respectively, and a total of 3,750 concatenations are used for testing.

In this study, we assume that melt pools in a concatenation formed under the same process parameters have consistent characteristics; then they are defined as a normal case. Otherwise, when a few melt pools in a sequence are different, it is defined as an anomalous case. Using this assumption, we defined normal inputs for the training set by excluding melt-pool concatenations with anomalous, melt pools like FIGURE 6. We also consider data augmentation to prevent overfitting and get more variety of dataset. The training set is geometrically transformed with two strategies: 1) Scaling up and down by where a range is [70% ,130%], and 2) Rotation where a range is [-2π, 2π]. The example images before and after data augmentation are shown in FIGURE 7.

3.3 Convolutional LSTM-Autoencoder Architecture

Based on the proposed approach, we design a ConvLSTM-Autoencoder (ConvLSTMAE) for the spatial-temporal modeling. The ConvLSTMAE consists of three networks: Encoder, Decoder, and latent space as shown in FIGURE 5. Encoder reduces the dimensions of the inputs of image concatenations into a latent space with convolutional layers and

FIGURE 6: EXAMPLES OF ANOMALOUS, MELT-POOL IMAGES

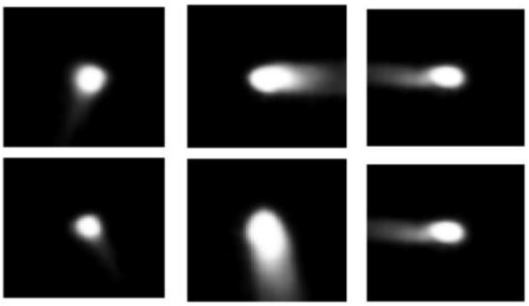

FIGURE 7: EXAMPLES OF MELT-POOL IMAGES. IMAGES AT THE TOP ARE BEFORE DATA AUGMENTATION, AND IMAGES AT THE BOTTOM ARE AFTER DATA AUGMENTATION.

TABLE 1: THE DETAIL OF CONVOLUTIONAL LSTM-AUTOENCODER ARCHITECTURE USED FOR THE MELT-POOL MODELING

Network	Layer	Channel (in/out)	Filter size	Stride	Activation
Encoder	*Conv2D_TimeDistributed*	1/128	(5,5)	2	*ReLU*
	Batch_Normalization	128/128	-	-	-
	Conv2D_TimeDistributed	128/64	(5,5)	2	*ReLU*
	Batch_Normalization	64/64	-	-	-
	ConLSTM2D	64/64	(3,3)	1	*ReLU*
	Batch_Normalization	64/64	-	-	-
latent space	*ConLSTM2D_TimeDistributed*	64/32	(3, 3)	1	*ReLU*
decoder	*ConLSTM2D_TimeDistributed*	32/64	(3, 3)	1	*ReLU*
	Batch_Normalization	64/64	-	-	-
	Conv2DTranspose_TimeDistributed	64/64	(5,5)	2	*ReLU*
	Batch_Normalization	64/64	-	-	-
	Conv2DTranspose_TimeDistributed	64/128	(5,5)	2	*ReLU*
	Batch_Normalization	128/128	-	-	-
	Conv2DTranspose_TimeDistributed	128/1	(2,2)	1	*Sigmoid*

recurrent LSTM layers. Decoder reconstructs the image sequence from the latent space with the reverse order of the Encoder's architecture. ReLU is used for a non-linear function and Batch normalization layer is added after ReLU to stabilize the weight updates. TABLE 1 shows the detail of ConvLSTMAE's architecture. Then, the reconstructed concatenations of melt-pool images ($\hat{x}$) are compared with the initial image concatenations (x), and a loss $L(x, \hat{x})$ between them is back-propagated to update the weights of the networks, aiming to minimize the loss. In this case, Binary Cross Entropy (BCE) is used as the loss L as shown in Equation (16):

$$L: BCELoss(x, \hat{x}) = -\frac{1}{N}\sum_{i=1}^{N} x_i ln\,(\hat{x}_i) \tag{16}$$

, where N denotes a batch size. Based on the validation set, the N is 32 and the epoch is 200 in this case study.

4 RESULTS AND DISCUSSION

We investigate an additional model, which is a Convolutional Autoencoder (ConAE), to compare the effect of the proposed, spatial-temporal modeling. A ConvAE architecture is referred to in [9] that dealt with the same issue but did not consider a temporal aspect in addition to its consideration of spatial data. The ConvAE's training settings are identical to those of ConvLSTMAE, however, its inputs are single, melt-pool images while not being structured based on the proposed approach. To monitor anomalies, Normalized Mean Square Error (NMSE) is used as the anomaly score. NMSE is defined as square error divided by the mean pixel intensity [3]. It can focus on reconstruction errors of melt pool sequence by minimizing the effect of melt-pool size. Equation (17) represents NMSE as follows:

$$NMES = \frac{1}{\underline{x}}\sum\left|\left|x - \hat{x}\right|\right|^2 \tag{17}$$

, where $\underline{x}$ means the mean pixel of x. A comparison with a monitoring chart of anomaly score on the testing set is shown in FIGURE 8. The top of FIGURE 8 depicts the case of ConvLSTMAE, whereas the bottom depicts the case of ConvAE. Each anomaly score threshold is computed from the 99th percentile of the training set's anomaly score, allowing an error of the selected training set.

To evaluate quantitatively the performance of two models, Accuracy, Precision, Recall, and F1 score, which are commonly used metrics for binary classification, are used. Each image in the testing dataset is labeled manually as "normal" and "anomalous". A total of 3,554 images are labeled as "normal", whereas a total of 196 images are labeled as "anomalous". The image sequence which includes at least one image with "anomalous" label is labeled as "anomalous". TABLE 2 shows a comparison between the performance of the ConvLSTMAE and the ConvAE on the testing set, which shows the proposed approach's outperformance.

TABLE 2: Performance measurement comparison

Model	Accuracy	Recall	Precision	F1-score
ConvAE	0.87	0.87	0.91	0.89
Conv LSTMAE	**0.98**	**0.98**	**0.98**	**0.98**

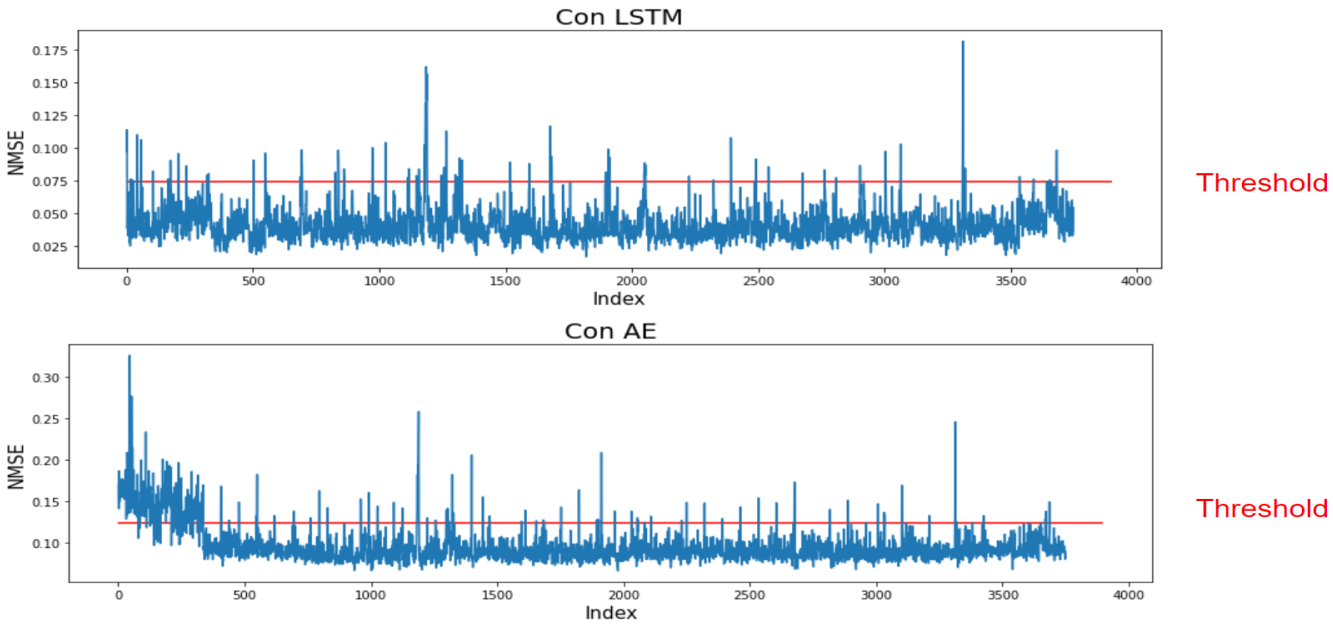

FIGURE 8: A COMPARISON BETWEEN THE CONVLSTMAE ENABLED BY THE PROPOSED APPROACH (TOP) AND A CONVENTIONAL CONVAE LACKING SPATIAL-TEMPORAL MODELING (BOTTOM) WITH A MONITORING CHART OF ANOMALY SCORE

5 CONCLUSION

In this paper, we proposed a novel approach of spatial-temporal modeling using DL for real-time monitoring of LPBF. The proposed approach represented in-situ, monitoring and control data of LPBF at multiple scales. Then, the approach extracted spatial-temporal relationships for in-situ monitoring of LPBF processes. Lastly, the approach presented a spatial-temporal, modeling method using the architecture of ConvLSTM to monitor the spatial-temporal relationships and detect anomalies. A case study developed a ConvLSTM-Autoencoder model using melt-pool images based on the proposed approach, which showed improved performance. The novel, data-driven approach improves spatial-temporal modeling of AM dynamics directly from real-time data for the monitoring of varying AM environments. In the future, we will fuse various real-time data at multiple, spatial-temporal scales.

ACKNOWLEDGEMENTS

No approval or endorsement of any commercial product by NIST is intended or implied. Certain commercial equipment, instruments or materials are identified in this report to facilitate better understanding. Such identification does not imply recommendations or endorsement by NIST nor does it imply the materials or equipment identified are necessarily the best available for the purpose.

REFERENCES

[1] Ko, H., Moon, S. K., and Hwang, J., 2015, "Design for additive manufacturing in customized products," International Journal of Precision Engineering and Manufacturing, 16(11), pp. 2369-2375.

[2] Ko, H., Yang, Z., Ndiaye, N. Y., Witherell, P., and Lu, Y., 2022, "A Framework driven by Physics-informed Machine Learning for Process-structure-property Causality Analytics in Additive Manufacturing," Journal of Manufacturing Systems, Submitted.

[3] Larsen, S., and Hooper, P. A., 2022, "Deep semi-supervised learning of dynamics for anomaly detection in laser powder bed fusion," Journal of Intelligent Manufacturing, 33(2), pp. 457-471.

[4] Spears, T. G., and Gold, S. A., 2016, "In-process sensing in selective laser melting (SLM) additive manufacturing," Integrating Materials and Manufacturing Innovation, 5(1), pp. 16-40.

[5] Moges, T., Ameta, G., and Witherell, P., 2019, "A Review of Model Inaccuracy and Parameter Uncertainty in Laser Powder Bed Fusion Models and Simulations," Journal of Manufacturing Science and Engineering, 141(4).

[6] Gou, Y., Zhang, T., Liu, J., Wei, L., and Cui, J. H., 2020, "DeepOcean: A General Deep Learning Framework for Spatio-Temporal Ocean Sensing Data Prediction," IEEE Access, 8, pp. 79192-79202.

[7] Cook, P. S., and Murphy, A. B., 2020, "Simulation of melt pool behaviour during additive manufacturing: Underlying physics and progress," Additive Manufacturing, 31, p. 100909.

[8] Lane, B., and Yeung, H., 2020, "Process Monitoring Dataset from the Additive Manufacturing Metrology Testbed (AMMT): Overhang Part X4," Journal of research of the National Institute of Standards and Technology, 125.

[9] Fathizadan, S., Ju, F., and Lu, Y., 2021, "Deep representation learning for process variation management in laser powder bed fusion," Additive Manufacturing, 42, p. 101961.